On the interaction between calcite and dolomite: Insights from gas and aqueous geochemistry and mineralogical characterization

Mathieu Debure, Catherine Lerouge, Fabienne Warmont, Laura Bocher, Mélanie Lundy, Benoît Madé, Sylvain Grangeon

On the interaction between calcite and dolomite: insights from gas and aqueous geochemistry and mineralogical characterization

Mathieu Debure[(1,1)], Catherine Lerouge[1], Fabienne Warmont[2], Laura Bocher[3], Mélanie Lundy[4], Benoît Madé[4], Sylvain Grangeon[1]

(1) BRGM – French Geological Survey - 45060 Orléans - France.

(2) ICMN - UMR 7374 CNRS, Université d'Orléans - 1b rue de la Férollerie CS 40059 - 45071 Orléans Cedex 2 - France.

(3) Laboratoire de Physique des Solides - CNRS UMR 8502 -, Université Paris-Sud XI - Bâtiment 510 – 91405 Orsay - France.

(4) Andra - 1 – 7 rue Jean Monnet - 92298 Châtenay-Malabry - France.

Abstract

The current models developed to determine the pore water chemistry of clayrocks consider that divalent cations such as Ca, Mg and Fe are controlled by equilibrium reactions with pure carbonates. However, the Ca/Mg ratios measured in pore water are not always in agreement with calculations. Here we investigated the interaction between synthetic calcite and natural dolomite at ambient temperature and at 80°C. Despite the fast equilibration of the concentration in solution (within weeks), the gaseous CO_2 continued to increase in the experiments after several months of reaction at ambient temperature while it reached a steady state at 80°C. The observations made at ambient temperature are apparently in conflict (metastable system). However, nanoscale characterizations proved to be useful to evidence the constant evolution of the minerals during the experiments. Indeed, local equilibrium in solution enabled the precipitation of secondary phases despite their undersaturation with respect to the bulk solution and the dissolution of pristine phases. These results suggest that the dissolution/precipitation kinetics are slow and ongoing despite the apparent stability of the system, something usually not considered in the prediction of sedimentary facies over a geological timescale.

***Keywords**: Calcite, dolomite, cathodoluminescence, traces elements, nanoscale, water/rock/gas interactions.*

[1]Corresponding author. E-mail address: m.debure@brgm.fr (M. Debure).

28 **Graphical abstract**

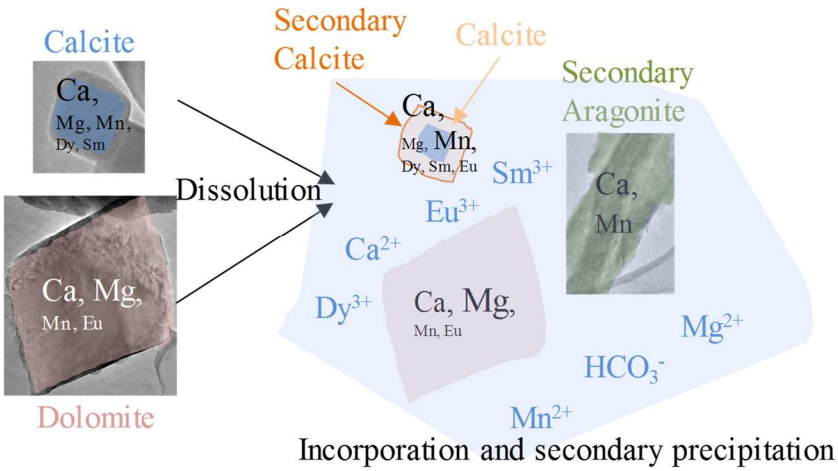

29

30

1. Introduction

The natural clay barriers targeted in the context of Carbon Capture and Storage (CCS) and at many potential nuclear waste disposal sites are clay formations deposited in marine conditions (Tournassat et al., 2007). The current geochemical models (Gailhanou et al., 2017; Gaucher et al., 2009; Pearson et al., 2011; Tremosa et al., 2012) consider that concentrations of divalent cations such as Ca, Mg and Fe in the pore water are driven by equilibrium reactions with pure carbonate minerals: calcite with Ca, dolomite with Mg and the couple siderite/goethite with Fe. Indeed, the almost systematic presence of carbonates in marine environments makes them good tracers for the chemical evolution of pore waters in sediments through geological times (Berner, 1980), based on the principle that diagenetic minerals have precipitated at equilibrium with local pore waters at a time t (Baker et al., 1982; Gaucher et al., 2009; Lerouge et al., 2013; Malone et al., 1990; Milesi et al., 2020; Morse and Mackenzie, 1990; Tosca and Wright, 2018; Wersin et al., 2016). This principle allows identifying the carbonates that are at equilibrium with present-day pore waters that are consequently, probably late diagenetic carbonates and carbonate grain rims in contact with interstitial waters. However, the observed and predicted Ca/Mg ratio in the pore water, with the assumption of equilibrium with calcite and dolomite, are in good agreement in the Callovian-Oxfordian (COx) clay rock (Lerouge et al., 2013) but not in the Opalinus clay (Jenni et al., 2014; Lerouge et al., 2014). Besides, petrological and chemical studies of carbonate minerals in these clay formations evidence several calcite generations, some of them related to the chemical evolution occurring during diagenesis (Lerouge et al., 2012; Lerouge et al., 2013). Such mineralogical and chemical complexity is currently not accounted for in geochemical modelling, but could explain some discrepancies.

An additional complexity in modeling the geochemical behavior of carbonate minerals such as calcite and dolomite results from the fact that, in their crystal structure, the cationic sites can incorporate several percent of foreign cations (e.g., Fe, Mn, Sr, Ba, Zn) by isomorphic substitution (Burton and Walter, 1991; Carpenter and Lohmann, 1992). Such change in crystal structure is likely to influence the dynamics and mechanisms of equilibrium between the solid and the solution and makes the study of the equilibrium between calcite, dolomite and the solution in terms of Ca/Mg activity ratio, ionic strength, available surface area, Mg and trace elements (Fe, Mn, Sr, Ba, Zn) content an inescapable step towards the understanding of the long term behavior of natural media.

In this regard, Mg, Mn, and Sr incorporation in calcite has been extensively studied. The main applications are the use of carbonate minerals as paleothermometers (Carpenter and Lohmann, 1992; Mangenot et al., 2018), the understanding of the inhibition of calcite growth (De Choudens-Sánchez and González, 2009; Deleuze and Brantley, 1997; Hong et al., 2016; Lopez et al., 2009; Mucci and Morse, 1983; Nindiyasari et al., 2015; Simkiss, 1964; Taft, 1967), and isotopic partitioning (Mavromatis et al., 2013). Although they are extremely useful, the fact that these studies are restricted to calcite means that they cannot be straightforwardly used for natural systems where calcite coexists with other carbonate minerals. To contribute to filling this gap, this study investigates the interaction between synthetic nanocrystalline calcite and natural dolomite in various solutions (pre-equilibrated water, NaCl 10^{-2} mol/L and ultrapure water) and at two temperatures, 25 °C and 80 °C. The overarching goal was to understand and quantify the calcite and dolomite interactions in aqueous systems. This was achieved by studying the water/rock/gas evolution and the distribution of trace elements in calcite using a multi-technique approach ranging from the macroscopic aqueous chemistry scale to the nanoscale.

2. Materials and methods

2.1. Synthetic calcite formation

The synthetic calcite was prepared according to the protocol previously published by Montes-Hernandez et al. (2007). Briefly, one liter of ultrapure water with an electrical resistivity of 18.2MΩ cm and 74.1 g $Ca(OH)_2$ (Sigma-Aldrich, 96% chemical purity) was placed in an autoclave (internal volume of 2 l). The hydroxide particles were immediately dispersed with mechanical agitation (400 rpm). The suspension was then heated to the target temperature (30 or 90 °C). Once the dispersion temperature had been reached, CO_2 (Linde Gas S.A.) was injected to reach a CO_2 partial pressure (pCO_2) of 55 bars (96.05 g at 30 °C and 80.18 g at 90 °C). The total pressure was then immediately adjusted to 90 bars by Ar injection, resulting in a vapor phase consisting mainly of an Ar + CO_2 mixture with the CO_2 in the gaseous state at 30 °C and the supercritical state at 90 °C. Sample purity was assessed using scanning electron microscopy and by powder X-ray diffraction (XRD).

2.2. Natural dolomite preparation

The natural dolomite was taken from the BRGM private collection. Powder (< 125 µm) was prepared by grinding and sieving monolithic dolomite blocks, and then cleaned ultrasonically in alcohol. The powder was dried and stored in a desiccator. The product was then analyzed by XRD, electron microprobe and bulk chemical analyses performed by inductively coupled plasma mass spectroscopy (ICP-MS). The content of major and trace elements is given in Table 1 and Supporting Information 1.

Table 1. Chemical composition of the minerals used in this study given in weight percent for major elements (QL: quantification limit, QL_{MgO} = 0.2 %); Trace elements are given in mg/kg with a quantification limit (QL) of 10 mg/kg for Ba and 0.01 mg/kg for the other traces.

Element	Units	Synthetic calcite	Natural dolomite
CaO	wt %	61.1	35.9
MgO	wt %	0.4	22.7
TIC	wt %	12.2	12.2
Total Fe (in Fe_2O_3)	mg/kg	346	233
MnO	mg/kg	86	25
Ba	mg/kg	<QL	1413
Sr	mg/kg	167	121
Dy	mg/kg	0.34	<QL
Eu	mg/kg	<QL	0.65
Sm	mg/kg	0.27	<QL

2.3. Experimental procedure

Two sets of batch equilibration experiments consisted of contacting calcite alone, dolomite alone, or calcite and dolomite with solutions of various chemical compositions at 25 and 80°C. Three solutions were used for the experiments: pure water, water with NaCl 0.01 M and water having a chemical composition calculated at equilibrium with calcite and dolomite. They were prepared with pure water (resistivity: 18.2 MΩ cm) and

analytical grade salts: NaCl, $MgCl_2:6H_2O$, $CaCl_2:2H_2O$, and $NaHCO_3$ (the detailed compositions of the solutions are given in the Table S2 and S3 in Supporting Information 1).

The first set of batch equilibration experiments (Table 2) were carried out in PTFE reactors, at 25 °C, in a glove box (Jacomex GT Concept T4 with O_2 content lower than 1 ppm) with 99%-N_2 / 1%-CO_2 atmosphere close to the gas equilibrium atmosphere calculated for storage conditions (Gaucher et al., 2009). In that case, the initial pressure and the partial pressure of CO_2 (pCO_2) were controlled by the glove box. In order to facilitate the characterization of calcite and dolomite at the end of experiments, calcite was kept isolated from dolomite placed with a dialysis membrane (threshold 3,500 Daltons) clamped with pliers, whereas dolomite was put directly in contact with the solution.. Before the experiments, the membranes were rinsed with pure water (resistivity: 18.2 MΩ cm) and placed overnight in a beaker filled with pure water. It was independently checked that no organic or inorganic carbon was released at this temperature by the dialysis membrane. During all the experiments, the solution with dolomite was stirred on a magnetic plate. There was no sampling during all these experiments.

The second set of batch experiments (Table 2) was carried out in stainless steel Berghof BR300 reactors at 25 and 80°C. Each reactor was equipped with a pressure gauge (0–10 bars with 0.1 % accuracy) and several gas and liquid sampling valves. The tank of the reactor contained a PTFE insert to prevent any chemical interactions between the steel container and the solution. For the experiments performed at 25 °C, the temperature was controlled by placing the reactors in a temperature-controlled chamber. For the experiments performed at 80°C (±2 °C), the reactor was placed on a heater and uniformly heated with a heating block made of Al. The temperature inside the reactor was 80 °C (±2 °C). The pressure inside the reactor was monitored continuously, in particular, to check for the absence of leakage. At 25°C, calcite was kept isolated from dolomite placed with a dialysis membrane (threshold 3,500 Daltons), again to facilitate the characterization of each mineral at the end of experiments when both calcite and dolomite are involved in the experiments. At 80 °C, calcite and dolomite were in direct contact as membrane degradation increased the CO_2 partial pressure. The solution was stirred to maintain its homogeneity during all the experiment. The device of the Berghof reactor allowed sampling, solutions and gases contrarily to the PTFE reactor. The sampling interval was redefined each time based both on the analysis of the results obtained during previous samplings and on the pressure remaining in the reactor.

At the end of all the experiments, the reactor was opened for solution and solid characterizations. All the solutions were filtered with 0.1 µm PVDF filters and the solids were freeze-dried before any characterization.

2.4. Analysis of the fluids: solutions and gases

The pH measurement of batch solutions was carried out with a Mettler Toledo Seven multi pH meter using NIST 4, 7 and 9 buffers. Cations (Ca^{2+}, Mg^{2+}, Sr^{2+}, Mn^{2+}, Na^{+}, Zn^{2+}, Ba^{2+} and total Fe) were analyzed in solution by inductively coupled plasma atomic emission spectroscopy (ICP-AES, Jobin Yvon) or by mass spectroscopy (ICP-MS, Thermo Fisher Scientific). Cl^- was analyzed by ionic chromatography (HPLC, Dionex). The typical uncertainty on aqueous concentrations was 3%. Alkalinity was measured using a Titrando 905 and a Dosino 800 equipped with a 5 mL syringe (Metrohm) to gradually inject an HCl solution (10^{-3} mol L^{-1}) into the sample. The alkalinity was calculated with the Gran method (Gran, 1952).

The gas (O_2, N_2 and CO_2) measurements were performed with a Varian star 3400 CX gas chromatograph (GC). To calculate the gas concentrations, the total pressure in the reactors was also measured. It is again stressed here that, for the experiments done at 80 °C, the reactors were maintained at this temperature in order to avoid any variation in pressure. Indeed, at 25 °C, the water saturation pressure is ~31 mbar (negligible as compared to the total pressure of > 1 bar) while, at 80 °C, the water saturation pressure is ~474 mbar. In addition, a misevaluation of the temperature by ± 1°C will lead to a 50 mbar pressure variation (Fig. S2 in Supporting Information 2). The value read on the pressure sensor of the reactor was systematically compared to the value obtained by GC. The relative evolution of both data was in good agreement, but the value given by the GC was systematically lower than the value given by the pressure sensor due to the gas expansion in the GC loop. Therefore, the CO_2 pressure in the reactors was calculated according to:

$$P_{CO_2} = \frac{(P_{sensor} - P_{satw})\frac{x_{CO_2 mes}}{100}}{P_{injection}} P_{sensor} \quad \textbf{(1)}$$

Where P_{sensor} is the pressure in bar in the reactor given by the sensor, P_{satw} is the water saturation pressure in bar at the reactor temperature, x_{CO2mes} is the quantity of CO_2 given by the GC in percent, $P_{injection}$ is the injection pressure in bar in the GC.

2.5. Characterization of the solid phases

The optical cathodoluminescence (CL) system used was a cold cathode from OPEA (Laboratoire Optique Electronique Appliquée, Fontenay-sous-Bois, France), mounted on an Olympus microscope, and operated at 15 kV, 400 µA. Data were recorded with a JVC KYF75U tri-CCD digital camera (Wayne, USA), with the gain set to 6 and laying time to 1. The three 12 mm-sized sensors had a resolution of 1024 pixels.

X-ray diffraction (XRD) measurements were carried out on bulk rock powder with a SIEMENS D8 X-ray diffractometer with CuKα radiation (λ = 1.5418 Å) operated at 40 kV and 40 mA. Samples were prepared using the RTS method (Zhang et al., 2003), and data were recorded in the 4-75 °2θ interval, with a counting time of 9 s per 0.029876° increment in 2θ. The ICDD references for the different minerals of relevance for the present study are quartz (00-046-1045), calcite (00-005-0586), dolomite (01-036-0426), and corundum (01-070-5679).

Infrared (IR) spectroscopy was performed with a Bruker Vertex 70 spectrometer. The Fourier-transformed IR (FTIR) spectra were recorded from 4000 to 400 cm^{-1} with a resolution of 2 cm^{-1}. Each value was the average of 100 acquisitions. Before each measurement, one reference spectrum was acquired in air and subtracted from the data. The samples were prepared by mixing 0.5 mg of powder sample and 150 mg of ground and previously dehydrated KBr (80 °C for 1 hour) and applying a 10 tons pressure for 1 min to form a pellet.

Chemical analyses of initial and final calcite and dolomite were performed on sample powders covered with a carbon coating, using a CAMEBAX SX50 electron probe micro-analyzer (EPMA - Genevilliers, France) with an accelerating voltage of 15 kV, a beam current of 12 nA, and a 1-2 µm beam diameter. The peak and background counting times were 10 s for Ca, Mg, Mn and Fe. The detection limits were 20 ppm for Ca, 8 ppm for Mg, 44 ppm for Mn and 40 ppm for Fe. The standards used included both well-characterized natural minerals and synthetic oxides. Matrix corrections were performed with a ZAF computing program (Merlet, 1994).

Transmission electron microscopy (TEM) observations were performed with a Philips CM20 equipped with a LaB_6 filament and coupled with EDX energy-dispersive X-ray spectrometry [Si(Li) detector], operated at 200 kV. Prior to observation, samples were dispersed in ultra-pure ethanol using an ultrasonic bath and then deposited on lacey carbon copper grids. In parallel, other calcite crystals were embedded in a LR-white resin and cut with a microtome to produce ~80 nm thick slices.

Finally, we performed nanoscale spatially-resolved (1 nm) cathodoluminescence (STEM-CL) under liquid nitrogen cooling in a dedicated scanning transmission electron microscope (STEM; VG HB501, Vacuum Generators, East Sussex, U.K.) at 60 keV with 20 pA of beam current using a liquid N_2-cooled specimen holder and a custom-built CL system (Zagonel et al., 2011). All STEM-CL spectra were calibrated in wavelength with a Hg spectrum acquired under the same experimental conditions. The cooling system prevented sample deterioration under the focused beam.

Vertex component analysis (VCA) was used for endmember extraction from hyperspectral data (Nascimento and Dias, 2005). The method assumes that the data is a linear mixture of pure components (spectra) with the presence of pure pixels in the data. The predefined number of pure components (2 to 4) was adjusted for each hyperspectral map acquired.

2.6. Saturation index calculation

Saturation indices were calculated with PHREEQC v3 (Parkhurst and Appelo, 1999, 2013). No secondary phases were excluded from the calculation. Two databases were compared for the calculations: the ThermoChimie (Giffaut et al., 2014) and Thermoddem (Blanc et al., 2012) databases. However, as the latter reproduced the CO_2 partial pressure in the experiments more accurately (data not shown), all the results presented were calculated with this database. However, it should be noted that, except for the gas composition in systems that were heated to 80 °C, both databases led to very similar results (data not shown).

Table 2. Experimental conditions applied in the calcite /dolomite equilibration tests in various environmental conditions. The initial solution compositions are given in the Table S4.

Experiments		Solution	Temperature	Duration	Reactor type	Mass of calcite	Mass of dolomite	Amount of solution	Solid to liquid ratio
			°C	month		g	g	ml	(kg L^{-1})
1	Cc	NaCl 0.01 M	25	6	Berghof	2.75	0	180	0.02
2	Dol	NaCl 0.01 M	25	6	Berghof	0	2.75	180	0.02
3	Cc, Dol	pure water	25	3	PTFE	0.15	0.16	40	0.01
4	Cc, Dol	NaCl 0.01 M	25	3	PTFE	0.16	0.16	40	0.01
5	Cc, Dol	equilibrated water	25	3	PTFE	0.16	0.16	40	0.01
6	Cc, Dol	equilibrated water	25	7	Berghof	2.76	2.79	180	0.03
7	Cc	NaCl 0.01 M	80	6	Berghof	2.74	0	180	0.02
8	Dol	NaCl 0.01 M	80	6	Berghof	0	2.76	181	0.02
9	Cc, Dol	equilibrated water	80	17	Berghof	2.8	2.88	180	0.03

3. Results

3.1. *Fluid analyses: solutions and gases*

The batch experiments in Berghof reactors allowed monitoring the evolution of the partial pressure of CO_2 (pCO_2) in the gas phase at equilibrium with solutions and solids with time. The pCO_2 evolution in experiments at 80 °C with pure calcite (Exp. 7) or pure dolomite (Exp. 8) had contrasting behavior as a function of time. In the Exp. 7, the pCO2 steadily increased from $10^{-3.9}$ bars (4.4 days of equilibration) to $10^{-3.3}$ bars (128 days). At longer equilibration time, steady-state was observed. In Exp. 8, the pCO_2 could only be detected sporadically during the first 150 days of the reaction and was under the detection limit (10^{-5} bars) at higher equilibration times. In the experiment at 80°C, where both calcite and dolomite were present (Exp. 9), a steady state was also observed. However, it was reached much more rapidly (7 days), and the pCO2 ($10^{-4.8}$) was significantly lower than in the experiments with pure minerals, yet closer to that of dolomite than calcite, in agreement with the measured HCO_3^- in solution (Table 3). To determine the influence of temperature, a similar experiment with calcite and dolomite was also conducted at 25 °C (Exp. 6). In this latter experiment, a steady state was never reached: pCO_2 increased steadily from $10^{-4.7}$ to $10^{-4.1}$ bars after 7 months of equilibration time (Fig. 1a). Note that this evolution could not be linked to a pH evolution, the latter being constant throughout the experiment.

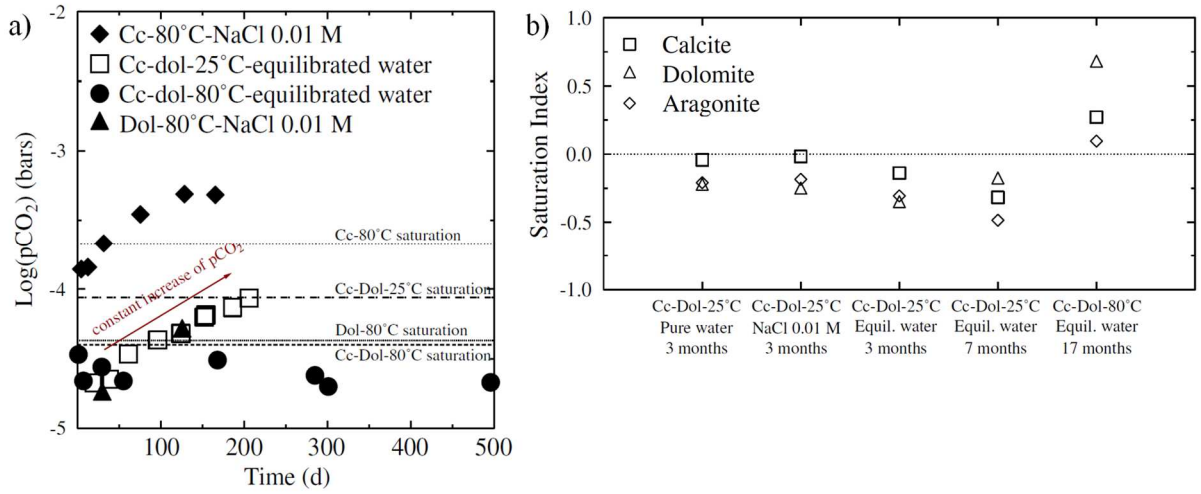

Fig. 1. Gaseous measurements and saturation indices (SI) from solution analyses. a): Evolution of the CO_2 partial pressure during the experiments Cc-dol-25°C-equilibrated water (Exp. 6), Cc-80°C-NaCl 0.01 M (Exp. 7), Dol-80°C-NaCl 0.01 M (Exp. 8) and Cc-dol-80°C-equilibrated water (Exp. 9). CO_2 was not measured in the experiments that lasted less than 7 months. b): Saturation indices of calcite, dolomite and aragonite in the experiments. The phases are close to equilibrium at 25 °C and oversaturated at 80 °C.

The solution chemistry was also investigated as a function of time to contribute to deciphering the mechanisms of calcite and dolomite reactivity from a solution chemistry point of view. Since the analysis of the pCO_2 as a function of time revealed that the equilibrium kinetics were much faster at 80 °C than at 25 °C, solution chemistry was not analyzed as a function of time for the experiments conducted at 80 °C, because the fast equilibration kinetics precluded the possibility of accurately sampling the solution during the equilibration step. After 3 months of reaction at 25 °C in PTFE reactors, the Ca concentrations in solutions are similar in

experiments 3, 4 and 5 [$(8.8 \pm 1.7)\times10^{-4}$ mol L^{-1}] where calcite and dolomite were present. This result is also observed for Mg concentrations [$(4.3 \pm 1.2)\times10^{-4}$ mol L^{-1}]. Therefore, despite a different initial composition, from 0 mol L^{-1} in pure water to 3.04 10^{-4} mol L^{-1} in pre-equilibrated water (Table 3 and Table S4 in the Supporting Information 1), the final concentrations of Ca and Mg in solution are similar in the three experiments. The concentration of trace elements that were initially present in the pristine minerals, were also comparable in all experiments. For example, Sr concentration in solution [$(9.3 \pm 0.8)\times10^{-7}$ mol L^{-1}] is similar in the three experiments, like Ba [$(1.3 \pm 0.1)\times10^{-5}$ mol L^{-1}] or Mn [$(8.7 \pm 1.7)\times10^{-8}$ mol L^{-1}] concentrations are. Contrastingly, after 7 months of reaction at 25 °C in the Berghof reactor (Exp. 6), all concentrations except for Mg and Sr were significantly different, suggesting a mechanism of reactivity with low kinetics (Table 3).

With the solution chemistry known, geochemical modeling, with the twofold aim to check for the consistency of aqueous chemistry data and gas composition and to determine whether the experiments reached thermodynamic equilibrium, can recalculate pCO2. In the two experiments in Berghof reactors in which calcite and dolomite were present at 25 °C (Exp. 6) and at 80 °C (Exp. 9), the calculated pCO_2 values were in good agreement with those measured after 7 months of equilibration at 25 °C or 17 months of equilibration at 80 °C. Two conclusions can be drawn from this result: first, there is a strong influence of temperature on the equilibration kinetics of the aqueous carbonate species/dissolved CO_2/atmospheric CO_2 system. Second, Exp. 6 at 25 °C and Exp. 9 at 80 °C are doubtlessly at thermodynamic equilibrium, and their study is thus relevant to the understanding of the calcite/dolomite system at equilibrium.

Finally, using solution and gas composition, the saturation indices of all minerals present in the thermodynamic database were checked to determine whether accessory phases could have possibly precipitated, and thus to provide constraints for the mineralogical study of the samples (Fig. 1b and Supporting Information 3). In all experiments, calcite and aragonite were predicted to be close to equilibrium, while vaterite was slightly undersaturated (Fig.S3 in Supporting Information 3). In the experiments conducted at 25 °C, the dolomite saturation index progressively increased with time, from -1.6 in the initial solution to -0.10 in Exp. 6, where it could thus be considered close to equilibrium. At 80 °C (Exp. 9), dolomite precipitation was predicted to be thermodynamically favored, since the saturation index was 0.6. Thermodynamic calculations also predicted the possible precipitation of secondary phases, namely magnesite (Fig.S3 in Supporting Information 3), but also ferrihydrite and other iron oxides such as goethite or hematite when Fe was detected in solution. This latter prediction is supported by our previous experiment which showed Fe oxide precipitation at the dolomite surface (Debure et al., 2017a). Note that other Mg-containing minerals that are reported to be of relevance for the study of the carbonate system (hydromagnesite, nesquehonite, lansfordite) (Urosevic et al., 2012) were unlikely to precipitate in our experimental conditions (SI < -3, not shown here).

252 ***Table 3. Solution composition at the end of the experiments (QL: quantification limit, QL_{Mg} = 2.5 10^{-5} mol L^{-1}, QL_{Fe} = 3.6 10^{-7} mol L^{-1}, QL_{Mn} = 1.8 10^{-9} mol L^{-1}, QL_{pCO2} =***
253 ***10^{-5} bars). All the pH values were measured at 25°C.***

254

Experiments		Initial solution	T	Time	Chemical composition of the final solution								
					final pH	Alkalinity	Ca	Mg	Sr	Fe	Ba	Mn	pCO_2**
			°C	month		Eq/L	mol/L	mol/L	mol/L	mol/L	mol/L	mol/L	bar
1	Cc	NaCl	25	6	11.12	$3.72\ 10^{-3}$	$5.59\ 10^{-4}$	< QL	$1.06\ 10^{-5}$	< QL	$2.75\ 10^{-7}$	< QL	< QL
2	Dol	NaCl	25	6	9.39	$1.08\ 10^{-3}$	$1.55\ 10^{-4}$	$1.28\ 10^{-4}$	$7.20\ 10^{-7}$	< QL	$1.48\ 10^{-5}$	$3.28\ 10^{-9}$	< QL
3	Cc, Dol	Pure water	25	3	7.59	$2.27\ 10^{-3}$	$1.07\ 10^{-3}$	$5.18\ 10^{-4}$	$9.78\ 10^{-7}$	< QL	$1.32\ 10^{-5}$	$1.04\ 10^{-7}$	n.d.
4	Cc, Dol	NaCl	25	3	8.07	$1.45\ 10^{-3}$	$7.24\ 10^{-4}$	$2.96\ 10^{-4}$	$9.79\ 10^{-7}$	< QL	$1.23\ 10^{-5}$	$7.17\ 10^{-8}$	n.d.
5	Cc, Dol	Equilibrated water	25	3	7.76	$1.91\ 10^{-3}$	$8.53\ 10^{-4}$	$4.85\ 10^{-4}$	$8.41\ 10^{-7}$	< QL	$1.23\ 10^{-5}$	$7.83\ 10^{-8}$	n.d.
6	Cc, Dol	Equilibrated water	25	7	8.63	$8.10\ 10^{-4}$	$1.92\ 10^{-4}$	$3.70\ 10^{-4}$	$1.43\ 10^{-6}$	< QL	$8.90\ 10^{-6}$	$6.92\ 10^{-9}$	$10^{-4.06}$
7	Cc	NaCl	80	6	9.88	$1.16\ 10^{-3}$	$3.27\ 10^{-4}$	$1.44\ 10^{-5}$	$6.63\ 10^{-6}$	$2.31\ 10^{-8}$	$2.23\ 10^{-7}$	< QL	$10^{-3.32}$
8	Dol	NaCl	80	6	8.47	$7.19\ 10^{-4}$	$2.37\ 10^{-4}$	$1.19\ 10^{-4}$	$1.05\ 10^{-6}$	$3.65\ 10^{-8}$	$1.62\ 10^{-5}$	$2.24\ 10^{-8}$	< QL
9	Cc, Dol	Equilibrated water	80	17	9.82	$6.01\ 10^{-4}$	$2.32\ 10^{-4}$	$9.05\ 10^{-5}$	$1.83\ 10^{-6}$	< QL	$1.13\ 10^{-5}$	$2.73\ 10^{-9}$	$10^{-4.88}$

255

256

257 * EW: pre-equilibrated water with calcite and dolomite, PW: pure deionized water, NaCl: 10^{-2} mol L^{-1} of NaCl salt.

258 ** n.d.: not determined as the reactors were not equipped with gas samplers

259

3.2. Solids characterizations

Pristine calcite occurs as 60-500 nm-sized euhedral grains (Fig. 2.a) while pristine dolomite measured 200 nm to 2 µm wide (Fig. 2.b). The pristine calcite had a dark blue intrinsic cathodoluminescence (CL) signal (Fig. 2.c), whereas natural dolomite had a red CL signal (Fig. 2.d) that was attributed to Mn incorporation at an Mg site (Gillhaus et al., 2000; Gillhaus et al., 2001). The luminescence of synthetic calcite grains after 3 months of reaction became yellow-orange in all the experiments (Fig. 2.e), indicating its reactivity by incorporating Mn or a dissolution/precipitation mechanism with Mn uptake in the structure of the secondary calcite. The yellow-orange color reveals Mn in the Ca position (yellow trend) and Mn in the Mg position (red trend) (Gillhaus et al., 2000; Gillhaus et al., 2010; Gillhaus et al., 2001). Some grains were yellow-green after 17 months at 80°C (Fig. 2.f) indicating either incorporation of rare earth elements (REE) or the precipitation of aragonite with Mn in its structure (Götte and Richter, 2009). However, this Mn incorporation was not quantified chemically and structurally by optical CL.

The structural formulas of calcite and dolomite, according to bulk chemical analyses performed by ICP-MS, (Table 1) were $CaMg_{0.009}Sr_{0.0002}Fe_{0.0001}Mn_{0.0001}Dy_{0.00002}Sm_{0.00002}C_{0.93}O_{2.9}$ (calcite) and $Ca_{0.57}Mg_{0.5}Ba_{0.0009}Sr_{0.001}Fe_{0.00006}Eu_{0.00004}Mn_{0.00003}C_{0.90}O_{2.9}$ (dolomite), and were consistent with STEM-CL results. Indeed, calcite had only one spectral component at ~400 nm that was intrinsic luminescence due to defects (Fig. 6.a), and dolomite had two components. The main one, at 650 nm, was due to Mn incorporation in the Mg position (Richter et al., 2003), and a minor one at ~400-450 nm was intrinsic luminescence (Kusano et al., 2014). A component at 580 nm, due to Mn incorporation in the Ca-position, was seldom observed (Supporting Information 4).

After reaction at 25 °C for 3 months, EPMA showed that most of the dolomite was enriched in Mg compared to the pristine sample while, conversely, calcite was depleted. The opposite trend was observed in the experiment performed at 80°C for 17 months (Fig. 3). Coherently, in the FTIR spectra (Fig. 4) collected on the samples taken from the experiments at 80 °C, the position of the calcite υ2 band was shifted towards higher wavenumbers as compared to that in the pristine calcite (Fig. 4.b), indicative of Mg incorporation (Lane and Christensen, 1997). However, no shift was observed for the data collected on the samples reacted at 25 °C, doubtlessly because of the lower degree of change in Mg abundance as compared to samples reacted at 80 °C (Fig. 4).

To gain better insights into the mechanisms of Mg enrichment or depletion, TEM experiments were performed on powders and microtome cuttings of calcite and dolomite that had reacted for the longest time at 80 °C (Exp. 9 after 17 months), because this sample was the closest to thermodynamic equilibrium (Fig. 1b). The morphologies of the calcite and dolomite grains were slightly modified (Fig. 7a) compared to pristine samples (Fig. 2a), as expected based on the fact that this experiment was performed in pre-equilibrated water. However, unexpectedly, several types of secondary phases were observed (Fig. 5.a and Fig.S5-1 and S5-2 in the Supporting Information 5). The first type of secondary phase was calcite and Mg-calcite, resembling crumpled sheets of paper and having a very limited thickness (Fig.S5-3.c). The second type had fibrous morphology (Fig.S5-2.d and e), and could be identified as dolomite (Fig.S5-2.f and g) and aragonite (Fig. 5.b and Fig.S5-1 and S5-2.h), which was a mineral predicted by thermodynamic calculations (Fig. 1b), observed and often found associated with dolomite (Fig. 5.b and Fig.S5-1).

298 Finally, to best understand the mechanisms of trace element transfer between calcite and dolomite, STEM-CL
299 experiments were conducted to determine if and how Mn, Eu, Dy, and Sm, that were initially present in calcite
300 (Dy, Sm) or dolomite (Eu), were transferred from one mineral to the other. In the experiment that lasted 3
301 months at 25°C (Exp. 3), Mn and Eu were incorporated in calcite (Fig. 6.a and c), but no uptake of Dy or Sm by
302 dolomite could be detected. Note that in this experiment, calcite morphology was modified and displayed
303 rounded forms characteristic of its dissolution because the solution was initially pure water. At 80 °C, after 17
304 months of interaction (Exp. 9), the revealed dolomite Mn content, inferred from the intensity of the band at 660
305 nm, decreased (Fig. 5.c). In contrast with the experiment conducted at 25 °C, Mn was not transferred to calcite,
306 but to the newly formed aragonite, as assessed from both spectral data (Fig. 5.d) and CL photomicrographs that
307 showed the presence of yellow-green component (Fig. 2.f). Calcite however incorporated Eu at the 0.25 µm
308 grain border (Fig. 7.d), while the signal collected on the core of the grains was dominated by calcite intrinsic
309 luminescence (Fig. 7.c).

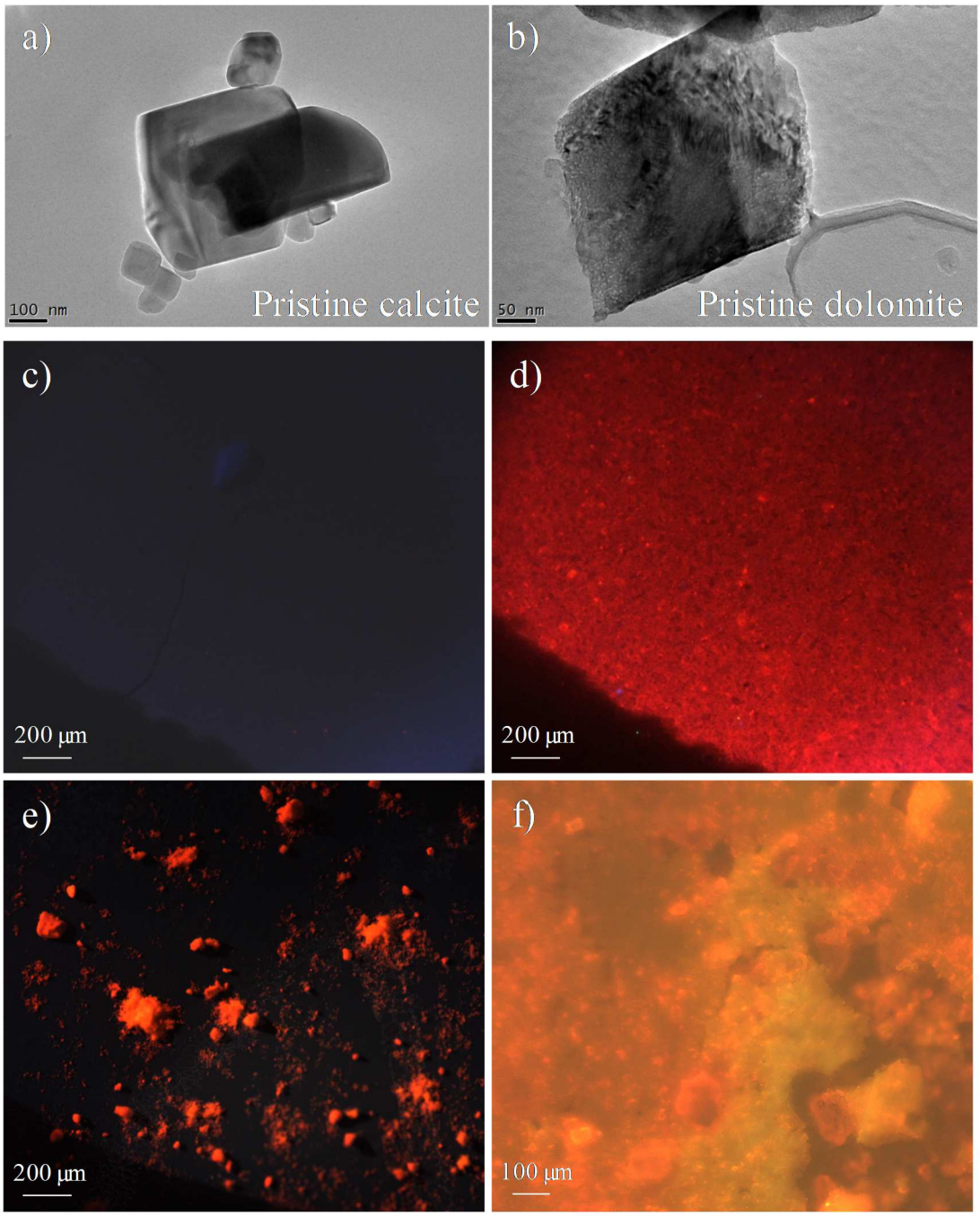

310

311 ***Fig. 2. TEM micrographs and CL photomicrographs of studied minerals; a): pristine calcite, b): pristine***
312 ***dolomite, c): dark blue synthetic calcite pellet (gain 6, laying time 1s), d): red natural dolomite pellet (gain 6,***
313 ***laying time 1s), e): experiment 3 final yellow-orange synthetic calcite powder after 3 months (gain 6, laying***
314 ***time 1s), f): experiment 9 final orange and yellow-green powder after 17 months (gain 6, laying time 0.5s)***

315

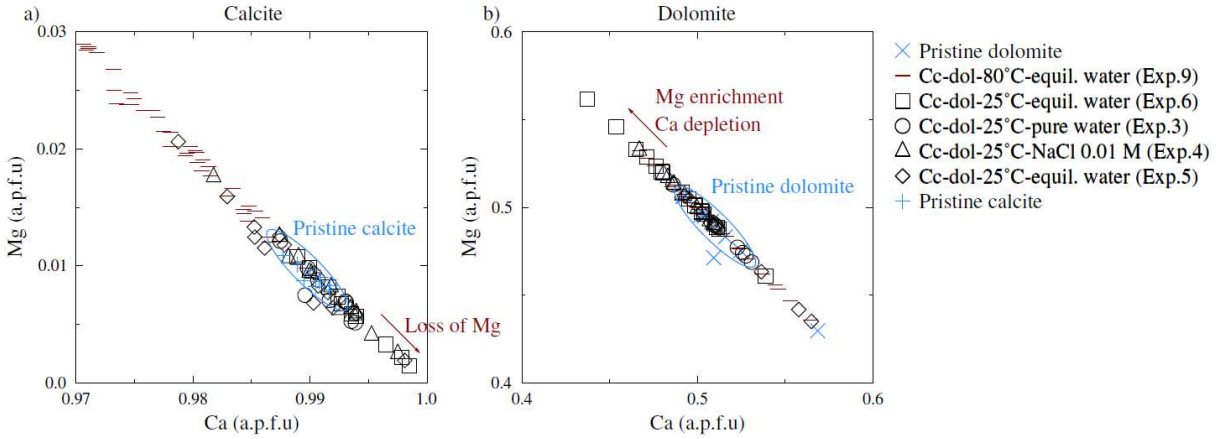

316

317 ***Fig. 3. EPMA analyses of pristine and reacted calcite and dolomite samples. a): calcite; b): dolomite. Calcite***
318 ***and dolomite were not separated in the experiment 9.***

319

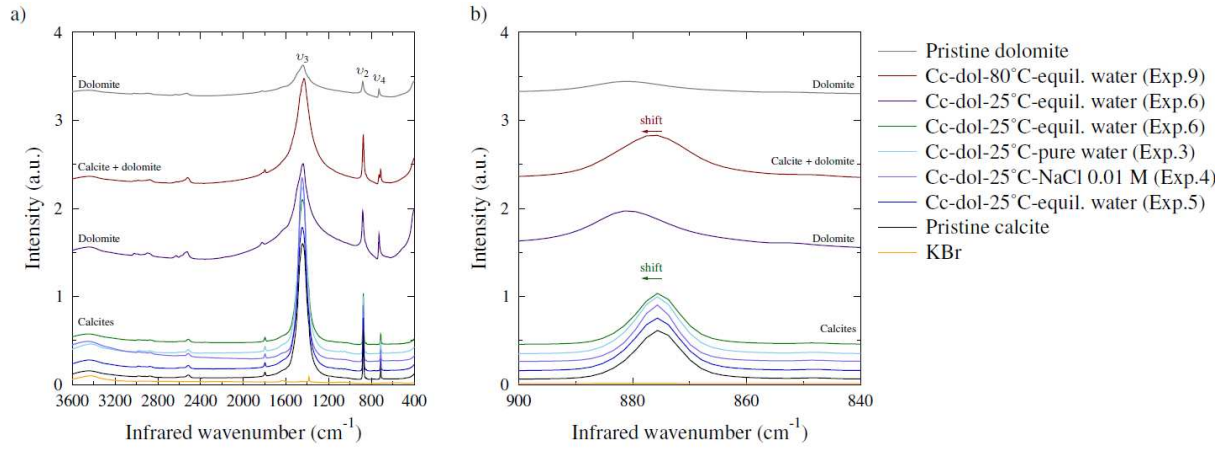

320

321 ***Fig. 4. IR spectrum of pristine and reacted calcite and dolomite samples. The calcite and dolomite v2, v3 and***
322 ***v4 vibration bands are distinguishable. a): the whole Infrared spectrum; b): focus on v2 vibration bands. The***
323 ***v4 vibration bands (focus not shown here) do not display a shift as observed for the v2 vibration bands in***
324 ***some experiments. For experiment 6, a membrane separated the minerals, on the graph both calcite and***
325 ***dolomite spectrum are given, therefore each curve is labelled "calcite" or "dolomite". For experiments 3, 4***
326 ***and 5, a membrane separated the minerals and only calcite spectra are showed on the figure. For experiment***
327 ***9, calcite and dolomite were mixed; so, the curve is labelled "calcite + dolomite" to highlight that the***
328 ***spectrum was not acquired on a single mineral.***

329

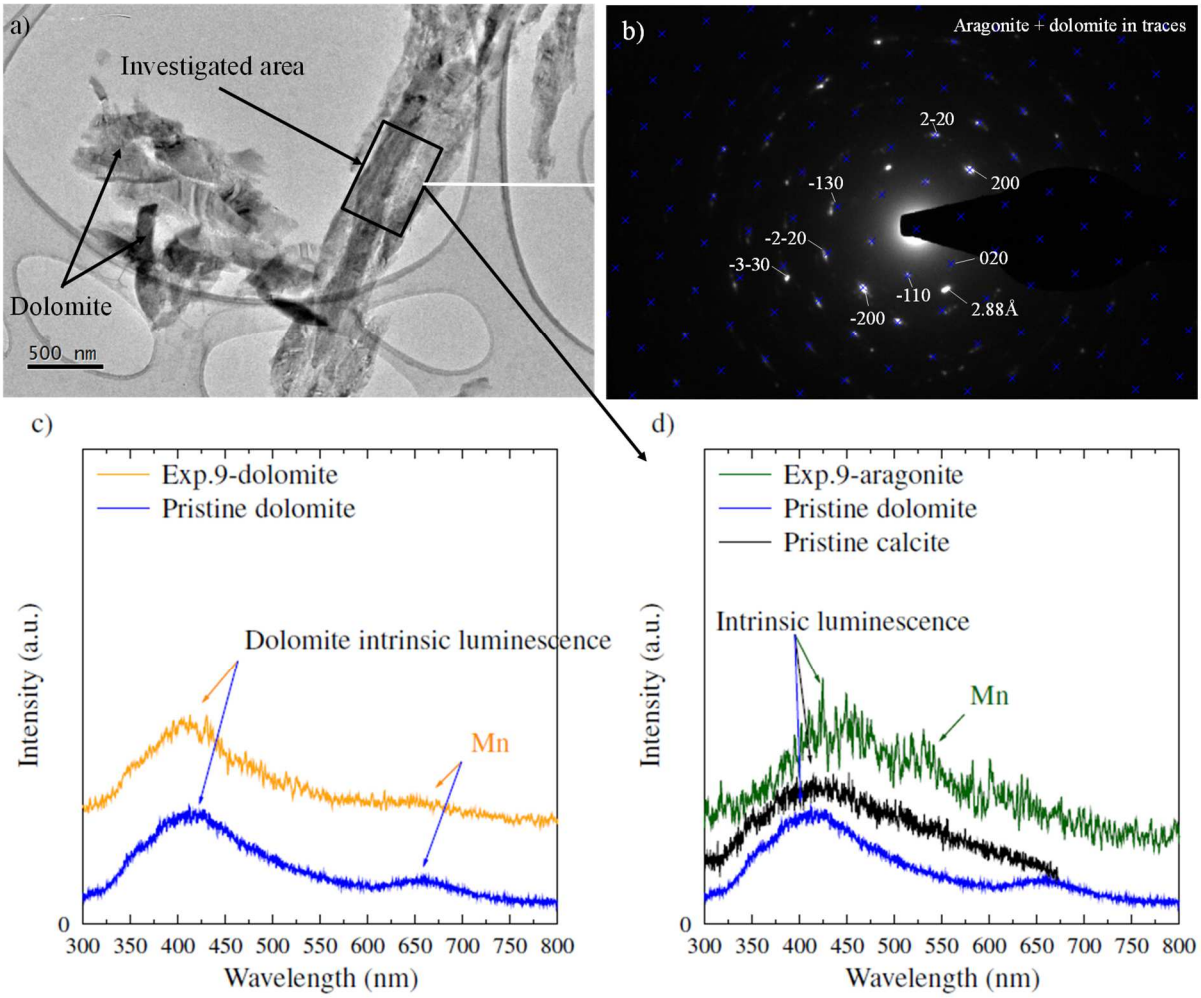

330

331 ***Fig. 5. TEM micrograph, diffraction pattern and STEM-CL results acquired for pristine dolomite and the***
332 ***experiment Cc-dol-80°C-equilibrated water (Exp. 9). a): Micrograph of several carbonates and secondary***
333 ***phases, b): Diffraction pattern of the secondary phases identified as aragonite and dolomite (EDX revealed 96***
334 ***At% of Ca and 4 At% of Mg); some crystallographic planes are given for aragonite and detailed in Fig.S5-1,***
335 ***the blue crosses represent the structural fit of aragonite performed with Crystbox software (Klinger and***
336 ***Jäger, 2015), the diffraction patterns that are not indexed are consistent with dolomite interplanar spacing***
337 ***(see Fig.S5-1 for SAED patterns without markings and other details); c): Comparison of spectral data on***
338 ***pristine dolomite and reacted dolomite displaying their intrinsic luminescence and Mn component, d):***
339 ***Comparison of spectral data acquired on aragonite displaying its Mn component with pristine calcite and***
340 ***dolomite.***

341

342

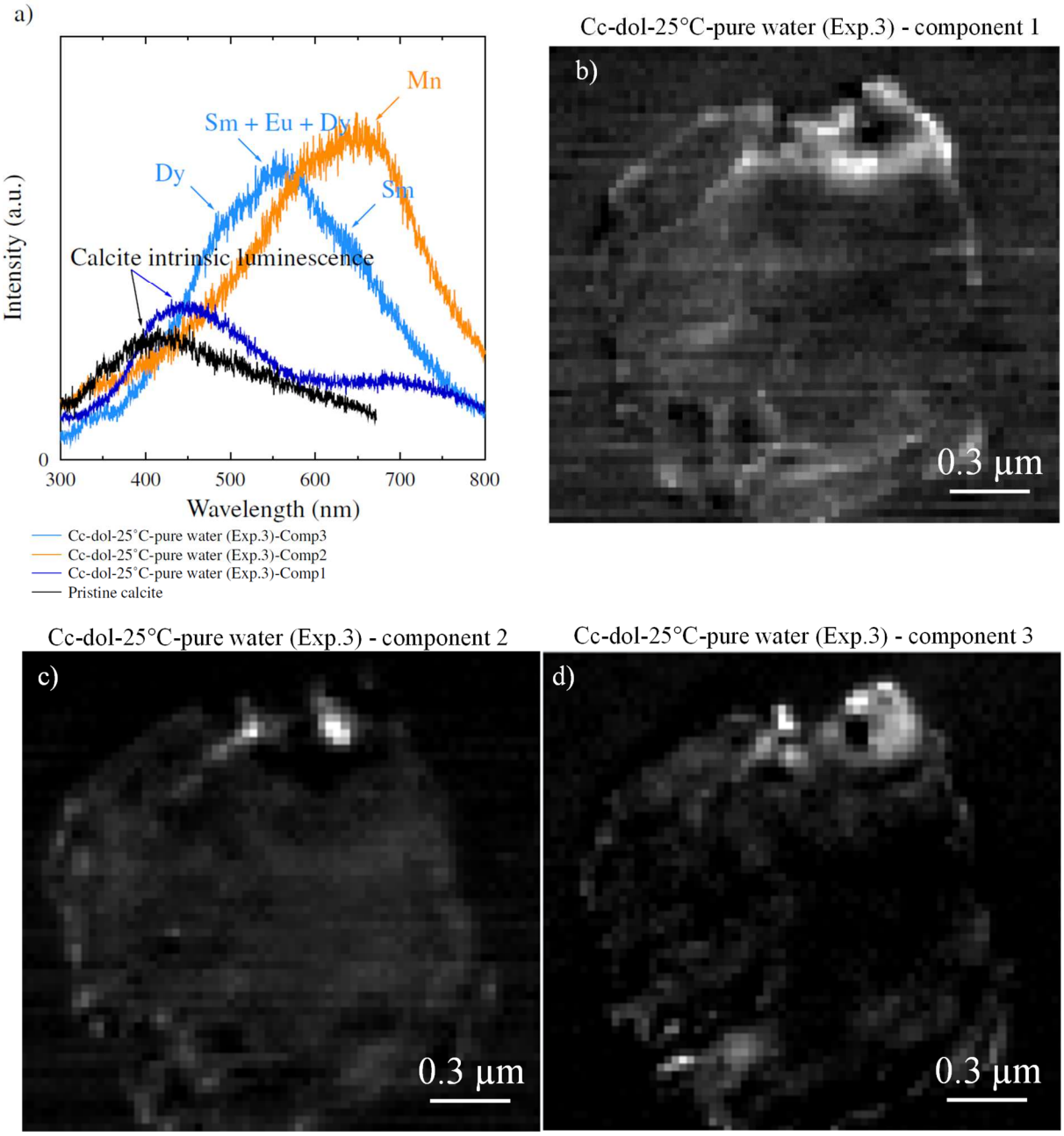

Fig. 6. STEM-CL results acquired on pristine calcite and calcite after 3 months of alteration (Exp. 3); a) spectral data on pristine calcite and on reacted calcite (component 1) displaying their intrinsic luminescence and additional spectral data on reacted calcite (component 2 and 3) revealing additional contribution due to trace incorporation, b), c) and d): maps of component 1, 2 and 3 identified by VCA.

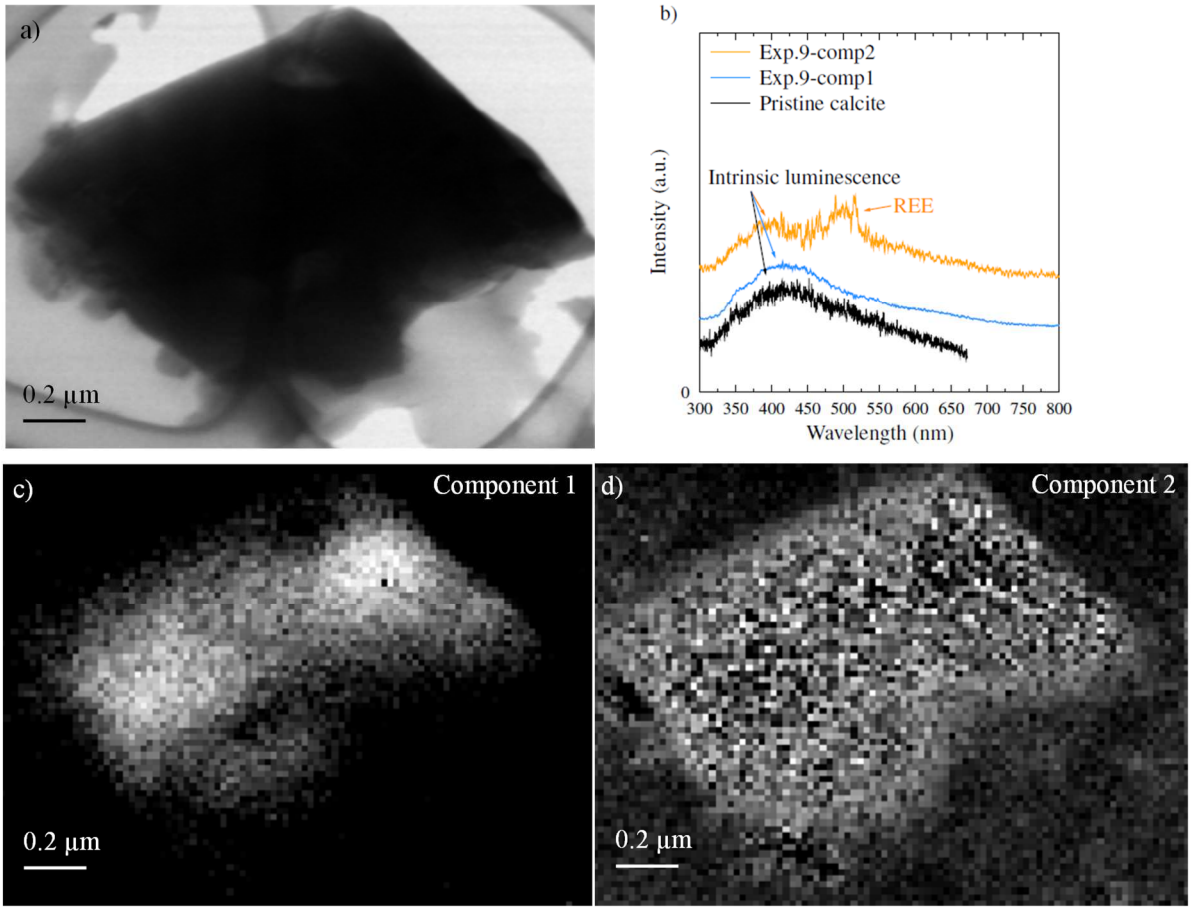

Fig. 7. Bright Field (BF) STEM-image and STEM-CL results acquired on calcite at the end of the experiment Cc-dol-80°C-equilibrated water (Exp. 9). a): BF, b): Comparison of spectral data on pristine calcite with those for reacted calcite displaying their intrinsic luminescence and REE component; c) and d): maps of component 1 and 2 identified by VCA.

4. Discussion

In laboratory experiments, when pure water is placed in contact with carbonate minerals, the aqueous concentration of dissolved species normally reaches steady state within 1-2 weeks (Debure et al., 2017b). Equilibrium is reached even faster if the solution is pre-equilibrated (using salts) to be at equilibrium with the mineralogical assemblage (calcite, dolomite or calcite/dolomite). However, even though aqueous chemistry quickly reaches a steady-state, the composition of the gas phase can still evolve after 200 days of reaction (Fig. 1), in apparent conflict with solution chemistry, and refer to the understanding of the interactions between rock, water and gas.

It was recently proposed that local equilibria at the solution/mineral interface might induce a dissolution/precipitation reaction without changing the bulk solution composition (Hellmann et al., 2015; Ruiz-Agudo et al., 2014; Ruiz-Agudo et al., 2012). For example, during dolomite dissolution, secondary phases can precipitate at the mineral surface while almost congruent dolomite dissolution still occurs (Debure et al., 2017a; Debure et al., 2017b; Urosevic et al., 2012). The slightly preferential Ca release, at short contact times (minutes

to hours), was attributed to a weakness of the Ca–O bond compared to the Mg–O bond (Busenberg and Plummer, 1982; Schott et al., 2009; Schott et al., 2012). This last result is directly linked to the strong tendency of Mg to replace Ca in the first calcite layers (Möller, 1973). From those observations, it appears that the solubility of carbonates is driven by the composition of their monomolecular surface layers which is in equilibrium with the solution (Möller and De Lucia, 2020). In these studies, due to the short contact time, the gas monitoring did not reveal any change between the beginning and the end of the experiments. However, over longer times, discrepancies occur (Fig. 1).

In the present study, and despite pre-equilibration, a constant solution composition was only reached after ~150 days, and it did not accurately match thermodynamic calculations (Fig. 8). Indeed, the latter was performed assuming that there were pure mineral phases and no kinetics whereas chemical composition and structure of the surface layer of carbonates can differ significantly from the bulk (Möller and De Lucia, 2020). Because the evolution of solution composition is related to mineralogical changes, it can be assumed that the exchange of chemical elements between mineralogical phases lasted at least ~150 days. For example, after 3 months of reaction at 25 °C, the Mg concentration increased at the dolomite surface while it decreased in calcite. This could be interpreted as Mg release during calcite dissolution and subsequent uptake by dolomite. However, since the initial solution was undersaturated with respect to both calcite and dolomite, both doubtlessly dissolved partially and released Ca and Mg in solution. Higher Mg sorption than Ca on the dolomite surface is unlikely according to the literature (Pokrovsky et al., 1999). Therefore, the remaining possible mechanisms are the precipitation of an Mg-rich phase (Urosevic et al., 2012) or a higher Ca release than Mg during dolomite dissolution (Schott et al., 2009; Schott et al., 2012).

In our case, a higher Ca release followed by secondary calcite formation (Pokrovsky et al., 1999) would explain both the apparent Mg enrichment of the dolomite and the apparent Mg depletion of the calcite. Moreover, the Mn released during the calcite and dolomite dissolution could precipitate in the newly formed calcite. Since calcite precipitation at the dolomite surface is unlikely (Berninger et al., 2017), it is proposed that the secondary calcite was formed at the surface of the pristine calcite grains and did not incorporate significant amounts of Mg. Indeed, this element acts as an inhibitor for calcite growth due to its incorporation in the crystal lattice that leads eventually to an increase of the solubility of calcite (Davis et al., 2000; Plummer and Mackenzie, 1974) and due to the exchange of Mg against Ca on the surface layers of calcite (Koss and Möller, 1974a; Morse et al., 1980). On the contrary, Fe and Mn decrease the solubility of calcite favoring its precipitation (Koss and Möller, 1974b). The CL (optic and STEM) results are consistent with two different mechanisms: at 25°C the reactions occur at the surface of the grains and are dominated by dissolution and precipitation (Fig. 6.c and d) while at 80°C an elemental diffusion from the surface to the center of the grains appears likely (Fig. 7.c and d). Note that this mechanism does not preclude the simultaneous precipitation of other secondary phases such as aragonite, which was observed after 17 months of interaction at 80 °C (Exp. 9). The fibrous shape of the secondary phases (Fig. 5.a) is consistent with fast crystallization in solution at low temperature.

The present results raise questions about the predominant mechanisms of carbonates' reactivity in sedimentary environments such as clay barriers investigated for toxic chemical retention (Debure et al., 2018; Gaucher et al., 2009; Markelova et al., 2018; Marty et al., 2018) or lacustrine carbonates investigated for paleoclimate recovery (Carpenter and Lohmann, 1992; Mangenot et al., 2018) and as potential hydrocarbon reservoir (Baker et al.,

1982; Chamley, 1989, 1997; Malone et al., 1990; Milesi et al., 2020; Milesi et al., 2019; Morse and Mackenzie, 1990; Weaver, 1989). Indeed, the study of the porewater chemistry and carbonate diagenesis is especially important to predict chemical variations in a rock formation. However, (Murray et al., 1980) and (Emerson et al., 1982) demonstrated that this approach is not always working, especially for deep-sea sediment pore waters, due to the solubility changes of carbonates with pressure and temperature. It has also kept in mind that diagenesis and potential fluid mixing modifies the pore waters collected that might be at ages of depositional conditions. However, in relevant environments, porewater chemistry remains useful to assess long-term equilibrium and to predict chemical variations in a rock formation that are not reachable in laboratory conditions. Although ions such as Mg and Ca are usually considered at equilibrium with pure carbonates in solution, their concentrations depend solely on the carbonates surface composition rather than their bulk composition (Möller and De Lucia, 2020), the former depending on the reactivity of the carbonates in their environment. In the present study, the mineral characterization pleads for nucleation and growth of secondary carbonates rather than element incorporation in the crystal lattice due to diffusion at 25 °C while both mechanisms occur at 80 °C. In addition, the elongated particles observed in this study are commonly observed in sedimentary environments (Davis et al., 2004; Mather et al., 2018) and are characteristic of Mg-rich centers (Shuster et al., 2018), the Mg ions cause step rounding and surface segmentation (Davis et al., 2004; Hong et al., 2016; Nyirő-Kósa et al., 2018). However, the Mg concentration is only one of the variable parameters (time, solution composition, temperature, microbial influence) that can affect the morphology of the precipitating carbonates (Kirkham and Tucker, 2018; Meldrum and Cölfen, 2008). Indeed, silicates and clays are known to enhance the nucleation of Mg-bearing carbonates (Cuadros et al., 2016; Díaz-Hernández et al., 2013; Nyirő-Kósa et al., 2018) even in soil and therefore at low temperature. Clay minerals surrounding neoformed dolomite crystals can act as a catalytic material in the process of incorporation of Mg into the structure of the rhombohedral carbonates (Díaz-Hernández et al., 2013). Indeed, in confined porous media, the transport of reacting material is a rate-determining process. Permeability and porosity are low in clays leading to slow water circulation. This phenomenon may create local oversaturation with respect to carbonates which promote the incorporation of Mg or another element available in the system (Mn, REE, …) into the structure of the neoformed carbonate (Debure et al., 2017a; Díaz-Hernández et al., 2013; Urosevic et al., 2012). In addition, the local oversaturation can promote as well the exchange between divalent cations and Ca and finally change the surface chemistry and structure of carbonates (Möller and De Lucia, 2020; Möller and Rajagopalan, 1972). The above-mentioned mechanisms are also one explanation for the coexistence of many carbonate minerals in sedimentary environments as well as in the experiments carried out in this study that are in apparent violation with Gibb's phase rule (Brätter et al., 1972; Möller and Rajagopalan, 1972). Therefore, in sedimentary environments, carbonates' reactivity will also depend on the surrounding mineral, especially silicates and clays, which will influence the processes highlighted in this study (nucleation, growth and incorporation due to local equilibrium). To understand and assess the reactivity of clay barriers such as those investigated for toxic chemical retention, reaction paths have to be studied at the nanoscale in the whole system.

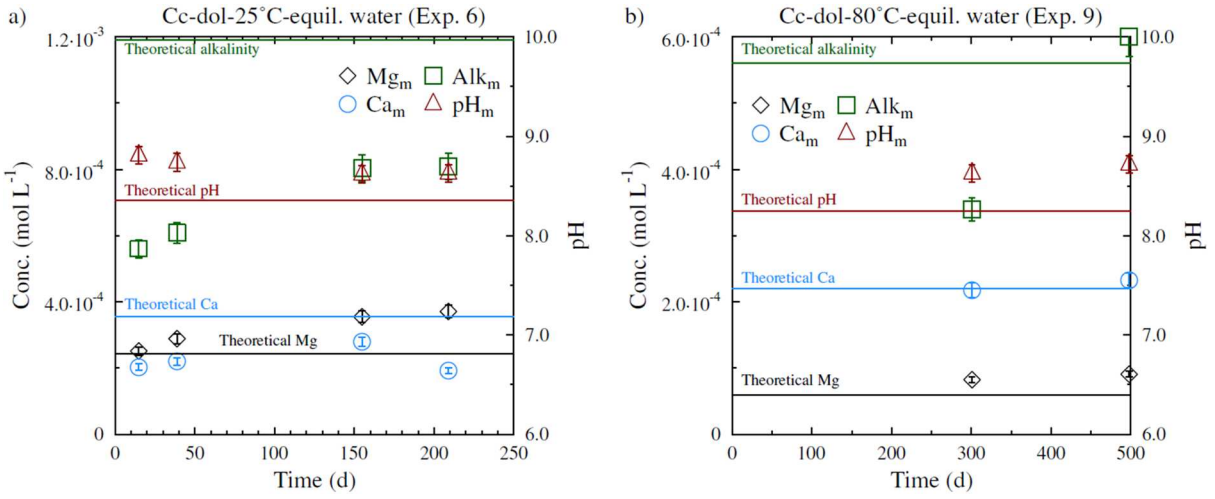

Fig. 8. Evolution of the aqueous species and pH and comparison with the theoretical values given by the calculation. a): Cc-dol-25°C-equilibrated water (Exp. 6), b): Cc-dol-80°C-equilibrated water (Exp 9). m: measured, lines represent the theoretical concentration in the experiments if the equilibrium is reached with the pure mineral assemblage.

5. Conclusion

The interaction between calcite and dolomite at ambient temperature and 80 °C results from an interplay of kinetics and local equilibrium. Despite the bulk solution steady state, the gas phase still evolved at ambient temperature while it reached a steady state at 80°C. This results in local equilibrium that was not achieved at ambient temperature. Indeed, secondary phases were observed to have precipitated in the bulk solution (e.g. aragonite) and at the calcite surface after initial dissolution. The surface precipitates were identified through nanoscale STEM-CL, following the Mn that was initially present in traces. The experiment revealed the constant transformation occurring during mineral interactions that can last for years. The reaction was identified only through advanced techniques or by waiting long enough and investigating higher temperature to increase the reaction rates. The understanding of such slow processes in porous media such as clays may ultimately be useful in the prediction of sedimentary facies over geological timescales.

Acknowledgements

This research has been financially supported by the ANDRA-BRGM scientific partnership. STEM-Cathodoluminescence and STEM-EELS analyses were conducted in the context of the METSA network. The authors thank G. Montes-Hernandez for providing the synthetic calcite samples.

Data availability

The datasets generated during the current study are available in the Supplementary Information or from the corresponding author upon reasonable request.

Competing interests

The authors declare no competing interests.

Additional information

Supplementary Information for this paper is available online.

References

Baker, P.A., Gieskes, J.M., Elderfield, H., 1982. Diagenesis of carbonates in deep-sea sediments; evidence from Sr/Ca ratios and interstitial dissolved Sr (super 2+) data. Journal of Sedimentary Research 52, 71-82.

Berner, R.A., 1980. Early diagenesis: a theoretical approach. Princeton University Press.

Berninger, U.-N., Saldi, G.D., Jordan, G., Schott, J., Oelkers, E.H., 2017. Assessing dolomite surface reactivity at temperatures from 40 to 120 °C by hydrothermal atomic force microscopy. Geochim. Cosmochim. Acta 199, 130-142.

Blanc, P., Lassin, A., Piantone, P., Azaroual, M., Jacquemet, N., Fabbri, A., Gaucher, E.C., 2012. Thermoddem: A geochemical database focused on low temperature water/rock interactions and waste materials. Appl. Geochem. 27, 2107-2116.

Brätter, P., Möller, P., Rösick, U., 1972. On the equilibrium of coexisting sedimentary carbonates. Earth and Planetary Science Letters 14, 50-54.

Burton, E.A., Walter, L.M., 1991. The effects of PCO2 and temperature on magnesium incorporation in calcite in seawater and MgCl2-CaCl2 solutions. Geochimica et Cosmochimica Acta 55, 777-785.

Busenberg, E., Plummer, L.N., 1982. The kinetics of dissolution of dolomite in CO 2 -H 2 O systems at 1.5 to 65 degrees C and O to 1 atm PCO 2. Am. J. Sci. 282, 45-78.

Carpenter, S.J., Lohmann, K.C., 1992. SrMg ratios of modern marine calcite: Empirical indicators of ocean chemistry and precipitation rate. Geochimica et Cosmochimica Acta 56, 1837-1849.

Chamley, H., 1989. Clay Minerals, Clay Sedimentology. Springer, pp. 3-20.

Chamley, H., 1997. Clay mineral sedimentation in the ocean, Soils and sediments. Springer, pp. 269-302.

Cuadros, J., Diaz-Hernandez, J.L., Sanchez-Navas, A., Garcia-Casco, A., Yepes, J., 2016. Chemical and textural controls on the formation of sepiolite, palygorskite and dolomite in volcanic soils. Geoderma 271, 99-114.

Davis, K.J., Dove, P.M., De Yoreo, J.J., 2000. The Role of Mg²⁺ as an Impurity in Calcite Growth. Science 290, 1134-1137.

Davis, K.J., Dove, P.M., Wasylenki, L.E., De Yoreo, J.J., 2004. Morphological consequences of differential Mg2+ incorporation at structurally distinct steps on calcite. American Mineralogist 89, 714-720.

De Choudens-Sánchez, V., González, L., 2009. Calcite and Aragonite Precipitation Under Controlled Instantaneous Supersaturation: Elucidating the Role of CaCO3 Saturation State and Mg/Ca Ratio on Calcium Carbonate Polymorphism. Journal of Sedimentary Research 79, 363 - 376.

Debure, M., Andreazza, P., Canizarès, A., Grangeon, S., Lerouge, C., Mack, P., Madé, B., Simon, P., Veron, E., Warmont, F., Vayer, M., 2017a. Study of Iron-Bearing Dolomite Dissolution at Various Temperatures: Evidence for the Formation of Secondary Nanocrystalline Iron-Rich Phases on the Dolomite Surface. ACS Earth and Space Chemistry 1, 442-454.

Debure, M., Montes-Hernandez, G., Lerouge, C., Madé, B., Tournassat, C., 2017b. Effect of Trace Elements on Carbonate Thermodynamic Constants. Procedia Earth and Planetary Science 17, 730-733.

Debure, M., Tournassat, C., Lerouge, C., Madé, B., Robinet, J.-C., Fernández, A.M., Grangeon, S., 2018. Retention of arsenic, chromium and boron on an outcropping clay-rich rock formation (the Tégulines Clay, eastern France). Science of The Total Environment 642, 216-229.

Deleuze, M., Brantley, S.L., 1997. Inhibition of calcite crystal growth by Mg2+ at 100°C and 100 bars: Influence of growth regime. Geochimica et Cosmochimica Acta 61, 1475-1485.

Díaz-Hernández, J.L., Sánchez-Navas, A., Reyes, E., 2013. Isotopic evidence for dolomite formation in soils. Chemical Geology 347, 20-33.

Emerson, S., Grundmanis, V., Graham, D., 1982. Carbonate chemistry in marine pore waters: MANOP sites C and S. Earth and Planetary Science Letters 61, 220-232.

Gailhanou, H., Lerouge, C., Debure, M., Gaboreau, S., Gaucher, E.C., Grangeon, S., Grenèche, J.M., Kars, M., Madé, B., Marty, N.C.M., Warmont, F., Tournassat, C., 2017. Effects of a thermal perturbation on mineralogy and pore water composition in a clay-rock: An experimental and modeling study. Geochimica et Cosmochimica Acta 197, 193-214.

Gaucher, E.C., Tournassat, C., Pearson, F.J., Blanc, P., Crouzet, C., Lerouge, C., Altmann, S., 2009. A robust model for pore-water chemistry of clayrock. Geochimica et Cosmochimica Acta 73, 6470-6487.

Giffaut, E., Grivé, M., Blanc, P., Vieillard, P., Colàs, E., Gailhanou, H., Gaboreau, S., Marty, N., Madé, B., Duro, L., 2014. Andra thermodynamic database for performance assessment: ThermoChimie. Appl. Geochem. 49, 225-236.

Gillhaus, A., Habermann, D., Meijer, J., Richter, D.K., 2000. Cathodoluminescence spectroscopy and micro-PIXE: combined high resolution Mn-analyses in dolomites – First results. Nuclear Instruments and Methods in Physics Research Section B: Beam Interactions with Materials and Atoms 161–163, 842-845.

Gillhaus, A., Richter, D.K., Götte, T., Neuser, R.D., 2010. From tabular to rhombohedral dolomite crystals in Zechstein 2 dolostones from Scharzfeld (SW Harz/Germany): A case study with combined CL and EBSD investigations. Sedimentary Geology 228, 284-291.

Gillhaus, A., Richter, D.K., Meijer, J., Neuser, R.D., Stephan, A., 2001. Quantitative high resolution cathodoluminescence spectroscopy of diagenetic and hydrothermal dolomites. Sedimentary Geology 140, 191-199.

Götte, T., Richter, D.K., 2009. Quantitative aspects of Mn-activated cathodoluminescence of natural and synthetic aragonite. Sedimentology 56, 483-492.

Gran, G., 1952. Determination of the equivalence point in potentiometric titrations. Part II. Analyst 77, 661-671.

Hellmann, R., Cotte, S., Cadel, E., Malladi, S., Karlsson, L.S., Lozano-Perez, S., Cabié, M., Seyeux, A., 2015. Nanometre-scale evidence for interfacial dissolution–reprecipitation control of silicate glass corrosion. Nat Mater 14, 307-311.

Hong, M., Xu, J., Teng, H.H., 2016. Evolution of calcite growth morphology in the presence of magnesium: Implications for the dolomite problem. Geochimica et Cosmochimica Acta 172, 55-64.

Jenni, A., Mäder, U., Lerouge, C., Gaboreau, S., Schwyn, B., 2014. In situ interaction between different concretes and Opalinus Clay. Physics and Chemistry of the Earth, Parts A/B/C 70–71, 71-83.

Kirkham, A., Tucker, M.E., 2018. Thrombolites, spherulites and fibrous crusts (Holkerian, Purbeckian, Aptian): Context, fabrics and origins. Sedimentary Geology 374, 69-84.

Klinger, M., Jäger, A., 2015. Crystallographic Tool Box (CrysTBox): automated tools for transmission electron microscopists and crystallographers. J Appl Crystallogr 48, 2012-2018.

Koss, V., Möller, P., 1974a. Oberflächenzusammensetzung, Löslichkeit und Ionenaktivitätsprodukt von Calcit in fremdionenhaltigen Lösungen. Zeitschrift für anorganische und allgemeine Chemie 410, 165-178.

Koss, V., Möller, P., 1974b. Surface ion exchange on calcite powder in the presence of Mn2+ ions. Inorganic and Nuclear Chemistry Letters 10, 849-854.

Kusano, N., Nishido, H., Inoue, K., 2014. Cathodoluminescence of calcite decomposed from dolomite in high–temperature skarn. Journal of Mineralogical and Petrological Sciences, 140612.

Lane, M.D., Christensen, P.R., 1997. Thermal infrared emission spectroscopy of anhydrous carbonates. Journal of Geophysical Research: Planets 102, 25581-25592.

Lerouge, C., Grangeon, S., Claret, F., Gaucher, E., Blanc, P., Guerrot, C., Flehoc, C., Wille, G., Mazurek, M., 2014. Mineralogical and isotopic record of diagenesis from the opalinus clay formation at benken, Switzerland: implications for the modeling of pore-water chemistry in a clay formation. Clays and Clay Minerals 62, 286-312.

561 Lerouge, C., Grangeon, S., Fléhoc, C., Buschaert, S., Mazurek, M., Matray, J.-M., Tournassat, C., 2012.
562 Diagenetic carbonates in clay-rich marine formations, International meeting "Clays in Natural and Engineered
563 Barriers for Radioactive Waste Confinement", Montpellier, France.

564 Lerouge, C., Vinsot, A., Grangeon, S., Wille, G., Flehoc, C., Gailhanou, H., Gaucher, E.C., Madé, B., Altmann,
565 S., Tournassat, C., 2013. Controls of Ca/Mg/Fe Activity Ratios in Pore Water Chemistry Models of the
566 Callovian-Oxfordian Clay Formation. Procedia Earth and Planetary Science 7, 475-478.

567 Lopez, O., Zuddas, P., Faivre, D., 2009. The influence of temperature and seawater composition on calcite
568 crystal growth mechanisms and kinetics: Implications for Mg incorporation in calcite lattice. Geochimica et
569 Cosmochimica Acta 73, 337-347.

570 Malone, M.J., Baker, P.A., Burns, S.J., Swart, P.K., 1990. Geochemistry of periplatform carbonate sediments,
571 Leg 115, Site 716 (Maldives Archipelago, Indian Ocean), Proceedings of the Ocean Drilling Program, Scientific
572 Results. Ocean Drilling Program, pp. 647-659.

573 Mangenot, X., Gasparrini, M., Gerdes, A., Bonifacie, M., Rouchon, V., 2018. An emerging thermochronometer
574 for carbonate-bearing rocks:Δ 47/(U-Pb). Geology 46, 1067-1070.

575 Markelova, E., Couture, R.-M., Parsons, C.T., Markelov, I., Madé, B., Van Cappellen, P., Charlet, L., 2018.
576 Speciation dynamics of oxyanion contaminants (As, Sb, Cr) in argillaceous suspensions during oxic-anoxic
577 cycles. Applied Geochemistry.

578 Marty, N.C., Lach, A., Lerouge, C., Grangeon, S., Claret, F., Fauchet, C., Madé, B., Lundy, M., Lagroix, F.,
579 Tournassat, C., 2018. Weathering of an argillaceous rock in the presence of atmospheric conditions: A flow-
580 through experiment and modelling study. Applied geochemistry 96, 252-263.

581 Mather, C.C., Skrzypek, G., Dogramaci, S., Grierson, P.F., 2018. Paleoenvironmental and paleohydrochemical
582 conditions of dolomite formation within a saline wetland in arid northwest Australia. Quaternary Science
583 Reviews 185, 172-188.

584 Mavromatis, V., Gautier, Q., Bosc, O., Schott, J., 2013. Kinetics of Mg partition and Mg stable isotope
585 fractionation during its incorporation in calcite. Geochimica et Cosmochimica Acta 114, 188-203.

586 Meldrum, F.C., Cölfen, H., 2008. Controlling Mineral Morphologies and Structures in Biological and Synthetic
587 Systems. Chemical Reviews 108, 4332-4432.

588 Merlet, C., 1994. An accurate computer correction program for quantitative electron probe microanalysis.
589 Microchim. Acta 114-115, 363-376.

590 Milesi, V.P., Debure, M., Marty, N.C.M., Capano, M., Jézéquel, D., Steefel, C., Rouchon, V., Albéric, P., Bard,
591 E., Sarazin, G., Guyot, F., Virgone, A., Gaucher, É.C., Ader, M., 2020. Early Diagenesis of Lacustrine
592 Carbonates in Volcanic Settings: The Role of Magmatic CO2 (Lake Dziani Dzaha, Mayotte, Indian Ocean).
593 ACS Earth and Space Chemistry 4, 363-378.

594 Milesi, V.P., Jézéquel, D., Debure, M., Cadeau, P., Guyot, F., Sarazin, G., Claret, F., Vennin, E., Chaduteau, C.,
595 Virgone, A., 2019. Formation of magnesium-smectite during lacustrine carbonates early diagenesis: Study case
596 of the volcanic crater lake Dziani Dzaha (Mayotte–Indian Ocean). Sedimentology 66, 983-1001.

597 Möller, P., 1973. Determination of the composition of surface layers of calcite in solutions containing Mg2+.
598 Journal of Inorganic and Nuclear Chemistry 35, 395-401.

599 Möller, P., De Lucia, M., 2020. The impact of Mg2+ ions on equilibration of Mg-Ca carbonates in groundwater
600 and brines. Geochemistry, 125611.

601 Möller, P., Rajagopalan, G., 1972. Cationic Distribution and Structural Changes of Mixed Mg—Ca Layers on
602 Calcite Crystals. Zeitschrift für Physikalische Chemie 81, 47-56.

603 Montes-Hernandez, G., Renard, F., Geoffroy, N., Charlet, L., Pironon, J., 2007. Calcite precipitation from CO2–
604 H2O–Ca(OH)2 slurry under high pressure of CO2. Journal of Crystal Growth 308, 228-236.

605 Morse, J.W., Mackenzie, F., T., 1990. Geochemistry of Sedimentary Carbonates. ELSEVIER, Amsterdam.

606 Morse, J.W., Mucci, A., Millero, F.J., 1980. The solubility of calcite and aragonite in seawater of 35%. salinity
607 at 25°C and atmospheric pressure. Geochimica et Cosmochimica Acta 44, 85-94.

608 Mucci, A., Morse, J.W., 1983. The incorporation of Mg2+ and Sr2+ into calcite overgrowths: influences of
609 growth rate and solution composition. Geochimica et Cosmochimica Acta 47, 217-233.

610 Murray, J.W., Emerson, S., Jahnke, R., 1980. Carbonate saturation and the effect of pressure on the alkalinity of
611 interstitial waters from the Guatemala Basin. Geochimica et Cosmochimica Acta 44, 963-972.

612 Nascimento, J.M.P., Dias, J.M.B., 2005. Vertex component analysis: a fast algorithm to unmix hyperspectral
613 data. IEEE Transactions on Geoscience and Remote Sensing 43, 898-910.

614 Nindiyasari, F., Griesshaber, E., Fernandez-Diaz, L., Astilleros, J.-M., Sanchez-Pastor, N., Ziegler, A., Schmahl,
615 W., 2015. The effect of Mg on the caracteristics of calcite crystal aggregates grown in biomimetic gelatin
616 hydrogel systems, Goldschmidt 2015, Prague.

617 Nyirő-Kósa, I., Rostási, Á., Bereczk-Tompa, É., Cora, I., Koblar, M., Kovács, A., Pósfai, M., 2018. Nucleation
618 and growth of Mg-bearing calcite in a shallow, calcareous lake. Earth and Planetary Science Letters 496, 20-28.

619 Parkhurst, D.L., Appelo, C.A.J., 1999. User's guide to PHREEQC (Version 2) - A computer program for
620 speciation, batch-reaction, one-dimensional transport, and inverse geochemical calculations. U.S. Geological
621 Survey, Denver, p. 312.

622 Parkhurst, D.L., Appelo, C.A.J., 2013. Description of Input and Examples for PHREEQC Version 3–a Computer
623 Program for Speciation, Batch-reaction, One-dimensional Transport, and Inverse Geochemical Calculations.
624 U.S. Geological Survey, Denver, p. 530.

625 Pearson, F.J., Tournassat, C., Gaucher, E.C., 2011. Biogeochemical processes in a clay formation in situ
626 experiment: Part E – Equilibrium controls on chemistry of pore water from the Opalinus Clay, Mont Terri
627 Underground Research Laboratory, Switzerland. Appl. Geochem. 26, 990-1008.

628 Plummer, L.N., Mackenzie, F.T., 1974. Predicting mineral solubility from rate data; application to the
629 dissolution of magnesian calcites. American Journal of Science 274, 61-83.

630 Pokrovsky, O.S., Schott, J., Thomas, F., 1999. Dolomite surface speciation and reactivity in aquatic systems.
631 Geochim. Cosmochim. Acta 63, 3133-3143.

632 Richter, D., Götte, T., Götze, J., Neuser, R., 2003. Progress in application of cathodoluminescence (CL) in
633 sedimentary petrology. Mineralogy and Petrology 79, 127-166.

634 Ruiz-Agudo, E., Putnis, C.V., Putnis, A., 2014. Coupled dissolution and precipitation at mineral–fluid interfaces.
635 Chemical Geology 383, 132-146.

636 Ruiz-Agudo, E., Putnis, C.V., Rodriguez-Navarro, C., Putnis, A., 2012. Mechanism of leached layer formation
637 during chemical weathering of silicate minerals. Geology 40, 947-950.

638 Schott, J., Pokrovsky, O.S., Oelkers, E.H., 2009. The Link Between Mineral Dissolution/Precipitation Kinetics
639 and Solution Chemistry. Reviews in Mineralogy and Geochemistry 70, 207-258.

640 Schott, J., Pokrovsky, O.S., Spalla, O., Devreux, F., Gloter, A., Mielczarski, J.A., 2012. Formation, growth and
641 transformation of leached layers during silicate minerals dissolution: The example of wollastonite. Geochimica
642 et Cosmochimica Acta 98, 259-281.

643 Shuster, A.M., Wallace, M.W., van Smeerdijk Hood, A., Jiang, G., 2018. The Tonian Beck Spring Dolomite:
644 Marine dolomitization in a shallow, anoxic sea. Sedimentary Geology 368, 83-104.

645 Simkiss, K., 1964. Variations in the Crystalline Form of Calcium Carbonate precipitated from Artificial Sea
646 Water. Nature 201, 492-493.

647 Taft, W., 1967. Carbonate Rocks. Elsevier, Amsterdam.

Tosca, N.J., Wright, V.P., 2018. Diagenetic pathways linked to labile Mg-clays in lacustrine carbonate reservoirs: a model for the origin of secondary porosity in the Cretaceous pre-salt Barra Velha Formation, offshore Brazil. Geological Society, London, Special Publications 435, 33-46.

Tournassat, C., Gaucher, E.C., Fattahi, M., Grambow, B., 2007. On the mobility and potential retention of iodine in the Callovian–Oxfordian formation. Physics and Chemistry of the Earth, Parts A/B/C 32, 539-551.

Tremosa, J., Arcos, D., Matray, J., Bensenouci, F., Gaucher, E.C., Tournassat, C., Hadi, J., 2012. Geochemical characterization and modelling of the Toarcian/Domerian porewater at the Tournemire underground research laboratory. Applied geochemistry 27, 1417-1431.

Urosevic, M., Rodriguez-Navarro, C., Putnis, C.V., Cardell, C., Putnis, A., Ruiz-Agudo, E., 2012. In situ nanoscale observations of the dissolution of dolomite cleavage surfaces. Geochim. Cosmochim. Acta 80, 1-13.

Weaver, C.E., 1989. Clays, muds, and shales. Elsevier.

Wersin, P., Mazurek, M., Mäder, U.K., Gimmi, T., Rufer, D., Lerouge, C., Traber, D., 2016. Constraining porewater chemistry in a 250 m thick argillaceous rock sequence. Chemical geology 434, 43-61.

Zagonel, L.F., Mazzucco, S., Tencé, M., March, K., Bernard, R., Laslier, B., Jacopin, G., Tchernycheva, M., Rigutti, L., Julien, F.H., Songmuang, R., Kociak, M., 2011. Nanometer Scale Spectral Imaging of Quantum Emitters in Nanowires and Its Correlation to Their Atomically Resolved Structure. Nano Letters 11, 568-573.

Supporting Information

Supporting Information 1 displays the initial solid and solution compositions. Bulk analyses performed after complete mineral dissolution. Supporting Information 2 shows the dependence of water saturation pressure on temperature over the investigated range. Supporting Information 3 gives additional saturation indices of other potential secondary phases that may precipitate in the experiments. Supporting Information 4 gives the cathodoluminescence spectral data acquired on pristine powders (calcite and dolomite). Supporting Information 5 shows micrographs and diffraction patterns of powders showing the alteration of pristine calcite and dolomite and the precipitation of secondary phase in the experiment Cc-dol-80°C-equil. water (Exp. 9).

List of Figures

List of Tables